

Joint Pilot Optimization, Target Detection and Channel Estimation for Integrated Sensing and Communication Systems

Zhe Huang, *Student Member, IEEE*, Kexuan Wang, An Liu, *Senior Member, IEEE*, Yunlong Cai, *Senior Member, IEEE*, Rui Du and Tony Xiao Han

Abstract

Radar sensing will be integrated into the 6G communication system to support various applications. In this integrated sensing and communication system, a radar target may also be a communication channel scatterer. In this case, the radar and communication channels exhibit certain joint burst sparsity. We propose a two-stage joint pilot optimization, target detection and channel estimation scheme to exploit such joint burst sparsity and pilot beamforming gain to enhance detection/estimation performance. In Stage 1, the base station (BS) sends downlink pilots (DP) for initial target search, and the user sends uplink pilots (UP) for channel estimation. Then the BS performs joint target detection and channel estimation based on the reflected DP and received UP signals. In Stage 2, the BS exploits the prior information obtained in Stage 1 to optimize the DP signal to achieve beamforming gain and further refine the performance. A Turbo Sparse Bayesian inference algorithm is proposed for joint target detection and channel estimation in both stages. The pilot optimization problem in Stage 2 is a semi-definite programming with rank-1 constraints. By replacing the rank-1 constraint with a tight and smooth approximation, we propose an efficient pilot optimization algorithm based on the majorization-minimization method. Simulations verify the advantages of the proposed scheme.

Index Terms

Integrated sensing and communication, Channel estimation, Target detection, Sparse Bayesian inference, Pilot design.

This work was supported in part by National Science Foundation of China (No.62071416), and in part by Huawei Technologies Co., Ltd. (Corresponding authors: An Liu.)

Zhe Huang, Kexuan Wang, An Liu and Yunlong Cai are with the College of Information Science and Electronic Engineering, Zhejiang University, Hangzhou 310027, China (email: anliu@zju.edu.cn).

Rui Du and Tony Xiao Han are with Huawei Technologies Co., Ltd. (email: tony.hanxiao@huawei.com).

I. INTRODUCTION

It is expected that future 6G communication system will integrate radar sensing and communication functions to support various important application scenarios, such as autonomous driving and smart cities [1]. Traditionally, radar sensing and communications are designed separately as independent systems, and they usually occupy different frequency bands to avoid interference. However, with the widespread application of the massive multiple input multiple output (MIMO) and millimeter wave (mmWave) communication technologies, future communication signals will have higher time and angle resolution, which makes it possible to use communication signals to achieve high-accuracy sensing. Therefore, integrated sensing and communication (ISAC), in which the radar sensing and communication sub-systems are jointly designed to simultaneously achieve high-speed communication and high-accuracy sensing using shared frequency band and hardware, has emerged as a key technology in future communication systems [1], [2], [3], [4]. Recently, ISAC has attracted tremendous research interest in both academia and industry [5], [6], [7], [8], [9]. For example, there have been an increasing number of works on ISAC, including the fundamental limits analysis [10], [11], transceiver architecture and frame structure [1], [9], ISAC waveform design [7], [12], [13], and temporal-spectral-spatial signal processing [6], [14], [15]. These works show that there exist complex interplays between radar sensing and communication. On the one hand, there is a tradeoff between radar sensing and communication since they have to compete for the same radio resource. On the other hand, radar sensing and communication may help each other by providing useful side information to each other and performing joint target detection and channel estimation.

In this paper, we focus on an interesting interplay between radar sensing and communication in massive MIMO ISAC system when the radar and communication channels exhibit certain joint burst sparsity, as illustrated in Fig. 1. Specifically, in many cases, some radar targets are also communication scatterers. As such, the angles of arrivals (AoAs) of the radar and communication channels partially overlap. Moreover, both radar targets and communication scatterers are usually concentrated in a few clusters, e.g., a large target/scatterer can be viewed as a cluster of point targets/scatterers. In this case, the AoAs of both radar and communication channels will concentrate on a few non-zero bursts [16]. Similar correlations between the radar and communication channels have also been reported in the literature. In [1], the communication scatterers are assumed to be part of the radar targets, and thus the AoAs of the communication

to address target detection and CE in massive MIMO ISAC system. In [1], the communication scatterers are assumed to be part of the radar targets. However, the channel estimation and target detection are performed separately based on the radar echo signal and channel estimation pilots, respectively. In [24], the authors proposed to obtain the partial CSI about the LoS path of the communication channel by using the BS as a radar to sense the position of each mobile user. Specifically, they proposed a two-stage target detection and CE scheme, in which the first stage performs target detection, and the second stage performs super-resolution estimation of the parameters associated with the radar target (i.e., the LoS path parameters of the user channel).

Pilot optimization for target detection: A few works have addressed the pilot optimization problem for target detection based on Cramer-Rao Bound (CRB). In [25], a single target detection problem has been considered and the pilot is optimized by minimizing the trace of the Cramer-Rao Matrix based on semi-definite relaxation (SDR). However, the SDR approach is only tight for some special cases such as single target detection but in general suffers from performance loss. In [26], the pilot has been optimized by minimizing the maximum eigenvalue of the Cramer-Rao Matrix, also through the SDR approach.

In the aforementioned studies, the radar target detection and communication CE are performed separately based on the radar echo signal and CE pilots, respectively. Moreover, it is very important to further enhance the performance of both radar sensing and communication CE in the low SNR regime in order to extend the coverage of ISAC systems, especially for high-frequency band with larger path loss. However, how to achieve high-accuracy radar sensing and CE in the low SNR regime remains a challenging problem. In this paper, we propose a two-stage joint pilot optimization, target detection and channel estimation (J-PoTdCe) scheme to fully exploit the pilot beamforming gain and joint burst sparsity of radar and communication channels for enhancing both the target detection and channel estimation performance in massive MIMO ISAC systems, especially for the low SNR regime. The main contributions are summarized below.

- **Two-stage J-PoTdCe scheme:** We propose a two-stage J-PoTdCe scheme so that the prior information obtained from Stage 1 can be used to optimize the pilots and refine the detection/estimation performance in Stage 2. Specifically, in Stage 1, the base station (BS) performs joint target detection and channel estimation based on the reflected omnidirectional DP and received UP signals. In Stage 2, the BS exploits the prior information obtained in Stage 1 to optimize the DP signal to further refine the performance.
- **Turbo-SBI algorithm:** We propose a hidden Markov model (HMM) to capture the joint

burst sparsity of the radar and communication channels. Based on this model, a Turbo Sparse Bayesian inference (Turbo-SBI) algorithm is proposed for joint target detection and channel estimation in both stages. Note that a Turbo-Orthogonal Approximate Message Passing (OAMP) algorithm has been proposed in [27] to exploit the joint burst sparsity of multi-user massive MIMO channels under partially orthogonal (PO) measurement/pilot matrix. In this paper, the associated measurement matrix is no longer PO because it contains optimized pilot matrix and dynamic AoA grid parameters for super-resolution AoA estimation. We show that the Turbo-OAMP can be viewed as an approximation of the proposed Turbo-SBI for PO measurement matrix.

- **Pilot optimization based on rank-1 approximation and majorization-minimization (MM):** The pilot optimization problem in Stage 2 is formulated as a semi-definite programming with rank-1 constraints, which aims at exploring the beamforming gain and minimizing the worst-case Cramer-Rao Bound (CRB) of the target parameters. By replacing the rank-1 constraint with a tight and smooth approximation, we propose an efficient pilot optimization algorithm based on the MM method. Compared with the conventional SDR algorithm in [25], [26], the proposed pilot optimization algorithm has similar complexity order but better performance since it directly takes into account the rank 1 constraints in the algorithm design.

Finally, the advantages of the proposed J-PoTdCe scheme and the associated Turbo-SBI and pilot optimization algorithms are verified by simulations under the clustered delay line (CDL) channel model in 3GPP R15 [28]. The rest of the paper is organized as follows. In Section II, we describe the system model and the overall two-stage J-PoTdCe scheme. In Section III, we present the Turbo-SBI algorithm for joint target detection and channel estimation in both stages. In Section IV, we present the CRB analysis and the pilot optimization algorithm in Stage 2. The simulation results and conclusions are given in Section V and VI, respectively.

II. TWO-STAGE J-POTDCE SCHEME

In this section, we describe the system model and the proposed two-stage J-PoTdCe scheme. Consider a TDD massive MIMO ISAC system with one BS serving a single-antenna mobile user while detecting K targets indexed by $k \in \{1, \dots, K\}$, as illustrated in Fig. 1. The BS is equipped with $M \gg 1$ antennas. In the channel estimation phase, we will focus on one single-antenna user for clarity. However, the proposed J-PoTdCe scheme can be readily extended to the

case with multiple multi-antenna users, by assigning orthogonal uplink pilots (UPs) for different antennas. While all targets reflect back the echo wave to the BS, not all of them contribute to communication paths between the BS and the user [1]. Therefore, it is natural to assume that there is a partial overlap between K targets and L communication scatterers. Note that we do not explicitly add clutters in the system model due to the following reasons. On one hand, the effects of weak clutters can be absorbed into the noise. On the other hand, the strong clutters can be treated as targets of non-interest, whose parameters will also be estimated to mitigate the interference caused by strong clutters and enhance the detection performance of the targets of interest. After detecting all the targets (interest or non-interest), the targets of interest can be further identified by exploiting the properties/features of their parameters. For ISAC systems, detecting the strong clutters may also help enhancing the channel estimation performance of the user because some strong clutters may also contribute to the communication paths.

A. Outline of the Two-Stage J-PoTdCe

In the two-stage J-PoTdCe scheme, the time axis is divided into frames, and each frame contains two phases: target detection and channel estimation phase and data transmission phase. In this paper, we will focus on the first phase, which can be further divided into the following two stages as shown in Fig. 2:

- Initial target detection and channel estimation (Stage 1): Stage 1 is to search for potential targets, and provide an initial estimation for the target parameters and communication channels. After Stage 1, the BS will have some prior information about the target/channel parameters, e.g., whether there is a target or communication scatterer in a certain direction. Such prior information can be exploited to optimize the pilots in the second stage. Specifically, the BS first sends P_1 omnidirectional DPs for initial target search. Then the user sends Q UPs to the BS for channel estimation. Finally, the BS performs the joint target detection and channel estimation based on the reflected DP and received UP signals.
- Refined target detection and channel estimation (Stage 2): Based on the prior information about the targets and channel obtained in the initial stage, the BS optimizes the pilots and sends P_2 directional DPs towards the targets and communication scatterers for more accurate observations. Finally, the BS refines the joint target detection and channel estimation based on the reflected DP signals in both stages as well as the UP signals in Stage 1.

Note that in the above descriptions, we have ignored the data transmissions for conciseness. In the frame structure in Fig. 2, the omnidirectional DPs in Stage 1 are actually transmitted at the end of the downlink subframe. Then the UPs in Stage 1 are transmitted at the beginning of the uplink subframe followed by the uplink data transmission. Finally, the DPs in Stage 2 are transmitted at the beginning of the next downlink subframe. Therefore, the channel and target parameters are assumed to be (approximately) constant with the duration of one subframe.

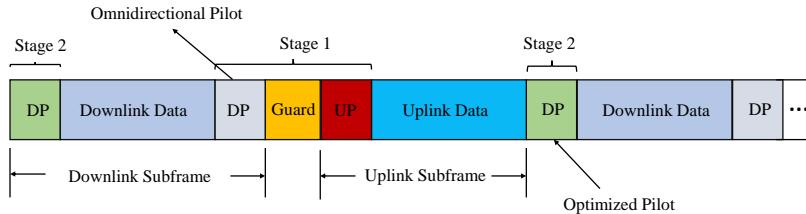


Fig. 2. Frame structure of the two-stage J-PoTdCe scheme.

B. Reflected DP Signal Model for Target Detection

In the p -th DP symbol duration of Stage t ($t \in 1, 2$), the BS transmits a DP $\mathbf{v}_{t,p} \in \mathbb{C}^M$, and the corresponding received signal can be expressed as

$$\mathbf{y}_{t,p}^r = \mathbf{H}^r \mathbf{v}_{t,p} + \mathbf{n}_{t,p}^r, \quad (1)$$

where $\mathbf{H}^r \in \mathbb{C}^{M \times M}$ is the radar channel matrix and $\mathbf{n}_{t,p}^r \sim \mathcal{CN}(0, (\sigma_n^r)^2 \mathbf{I}) \in \mathbb{C}^M$ is the additive white Gaussian noise (AWGN) with variance $(\sigma_n^r)^2$. For convenience, define the aggregate received DP signal (radar measurements) of all the P_t pilot symbols as $\mathbf{y}_t^r \triangleq [(\mathbf{y}_{t,1}^r)^T, \dots, (\mathbf{y}_{t,P_t}^r)^T]^T \in \mathbb{C}^{P_t M \times 1}$. The radar channel matrix depends on the AoAs and radar cross sections (RCSs) of the targets and can be modeled as

$$\mathbf{H}^r = \sum_{k=1}^K x_k^r \mathbf{a}(\theta_k^r) \mathbf{a}^H(\theta_k^r), \quad (2)$$

where θ_k^r and x_k^r are the AoA and RCS of the k -th target, $\mathbf{a}(\theta) \in \mathbb{C}^M$ is the array response vector for the BS antenna array. For a half-wavelength space uniform linear array (ULA), the array response vector is given by

$$\mathbf{a}(\theta) = \frac{1}{\sqrt{M}} [1, e^{-j\pi \sin \theta}, \dots, e^{-j(M-1)\pi \sin \theta}]^T.$$

C. Received UP Signal Model for Channel Estimation

In the q -th UP symbol duration of Stage 1, the user transmits an uplink pilot $u_q \in \mathbb{C}$ and the corresponding received signal can be expressed as

$$\mathbf{y}_q^c = \mathbf{h}^c u_q + \mathbf{n}_q^c, \quad (3)$$

where $\mathbf{h}^c \in \mathbb{C}^M$ is the communication channel vector and $\mathbf{n}_q^c \sim \mathcal{CN}(0, (\sigma_n^c)^2 \mathbf{I}) \in \mathbb{C}^M$ is the AWGN. For convenience, define the aggregate received UP signal (channel measurements) of all the Q pilot symbols as $\mathbf{y}^c \triangleq [(\mathbf{y}_1^c)^T, \dots, (\mathbf{y}_Q^c)^T] \in \mathbb{C}^{QM \times 1}$. The communication channel vector can be modeled as

$$\mathbf{h}^c = \sum_{l=1}^L x_l^c \mathbf{a}(\theta_l^c), \quad (4)$$

where θ_l^c and x_l^c are the AoA and complex gain of the l -th channel path, respectively.

Note that for clarity, we focus on a narrowband ISAC system with low-speed targets and users in this paper. In a wideband ISAC system with range and/or Doppler estimation capability, the model in (2) and (4) should also include the range/delay and Doppler of the targets/channel paths. Typically, in these ISAC systems, the estimation for the direction (AoA), range and Doppler of the targets/channel paths is implemented by processing the receiving channels over time and obtaining multi-channel measurements for each considered range-Doppler bin [29]. The model in (2) and (4) refers to a single range-Doppler bin [29]. Therefore, the joint target detection and channel estimation algorithm in this paper can be applied to detect/estimate multiple targets/channel paths for each range-Doppler bin in a wideband ISAC system.

To complete the proposed two-stage J-PoTdCe scheme, we need to design the joint target detection and channel estimation algorithm for both stages, as well as the pilot optimization algorithm in Stage 2, which will be elaborated in Section III and IV, respectively.

III. JOINT TARGET DETECTION AND CHANNEL ESTIMATION ALGORITHM

A. Sparse Angular Domain Channel with Dynamic Grid

We first describe the sparse angular domain representation for the radar and communication channels, which is a necessary step in order to apply the sparse recovery methods such as sparse Bayesian inference. One commonly used method to obtain a sparse representation of the channel is to define a uniform grid $\{\bar{\theta}_1, \dots, \bar{\theta}_{\widetilde{M}}\}$ of $\widetilde{M} \gg K + L$ AoA points, such that $[\sin \bar{\theta}_1, \dots, \sin \bar{\theta}_{\widetilde{M}}]$ is uniformly spaced over $[-1, 1]$. If the AoAs of the targets and channel paths indeed take values

in the discrete set $\{\bar{\theta}_1, \dots, \bar{\theta}_{\widetilde{M}}\}$, the radar and communication channels in (2) and (4) can be rewritten as

$$\mathbf{H}^r = \mathbf{A} \text{Diag}(\mathbf{x}^r) \mathbf{A}^H = \sum_{m=1}^{\widetilde{M}} x_m^r \mathbf{a}(\bar{\theta}_m) \mathbf{a}^H(\bar{\theta}_m), \quad (5)$$

$$\mathbf{h}^c = \mathbf{A} \mathbf{x}^c = \sum_{m=1}^{\widetilde{M}} x_m^c \mathbf{a}(\bar{\theta}_m), \quad (6)$$

where $\mathbf{A} \triangleq [\mathbf{a}(\bar{\theta}_1), \dots, \mathbf{a}(\bar{\theta}_{\widetilde{M}})]$ is a fixed array response matrix corresponding to the uniform grid, x_m^r is the radar cross section(RCS) of the target in the m -th AoA direction $\bar{\theta}_m$, and x_m^c is the complex gain of the channel path from the user to the m -th AoA direction $\bar{\theta}_m$ at the BS. For convenience, we define $\mathbf{x}^r \triangleq [x_1^r, \dots, x_{\widetilde{M}}^r]^T \in \mathbb{C}^{\widetilde{M}}$ as the angular domain radar channel, and $\mathbf{x}^c \triangleq [x_1^c, \dots, x_{\widetilde{M}}^c]^T \in \mathbb{C}^{\widetilde{M}}$ as the angular domain communication channel. If there is no target (active channel path) in the m -th AoA direction, we have $x_m^r = 0$ ($x_m^c = 0$). Therefore, there are K (L) non-zero elements in \mathbf{x}^r (\mathbf{x}^c) corresponding to the K targets (L active channel paths). Note that, we use x_m^r and x_m^c to denote the RCS of the target and complex channel gain in the m -th AoA direction, respectively, even though x_k^r and x_l^c have been used to denote the RCS of the k -th radar target and complex gain of the l -th active channel path in Section II.

In practice, however, the true AoA may not lie exactly on the \widetilde{M} discrete AoA grid points. As a result, we need to use a very large \widetilde{M} in order to achieve a high AoA estimation accuracy, leading to a high computational complexity. To overcome the above mismatch and complexity issues of using a fixed grid, we adopt dynamic grid parameters $\boldsymbol{\theta} \triangleq [\theta_1, \dots, \theta_{\widetilde{M}}]^T$. In this case, as long as $\widetilde{M} \geq K + L$, there always exist a set of unknown (and potentially non-uniform) grid parameters $\boldsymbol{\theta}$ that can exactly represent the true radar and communication channels by

$$\mathbf{H}^r = \mathbf{A}(\boldsymbol{\theta}) \text{Diag}(\mathbf{x}^r) \mathbf{A}(\boldsymbol{\theta})^H,$$

$$\mathbf{h}^c = \mathbf{A}(\boldsymbol{\theta}) \mathbf{x}^c,$$

where $\mathbf{A}(\boldsymbol{\theta}) \triangleq [\mathbf{a}(\theta_1), \dots, \mathbf{a}(\theta_{\widetilde{M}})]$. However, if we set $\widetilde{M} = K + L$ exactly, the likelihood function associated with the estimation of the dynamic grids $\boldsymbol{\theta}$ will have many local maxima, making it difficult to obtain an accurate estimation of $\boldsymbol{\theta}$ using the maximum likelihood (ML) method, as the algorithm can easily get stuck in a “bad” local maxima. If \widetilde{M} is sufficiently large, then by using a uniform grid as the initial point for $\boldsymbol{\theta}$, each true AoA will be very close

to one initial grid point, making it much easier for the algorithm to find a near-optimal solution for the ML estimation problem. In the rest of the paper, we set $\widetilde{M} = M$ to achieve a good tradeoff between the AoA estimation performance and complexity, since the AoA resolution for a massive MIMO array with $M \gg 1$ is roughly $O\left(\frac{1}{M}\right)$.

One may argue that when $\widetilde{M} = M$, the total number of radar and channel measurements $M(P_1 + P_2 + Q)$ is no less than the total number of parameters $3M$, and thus there is no need to use sparse recovery methods. However, a properly designed sparse recovery algorithm can fully exploit the joint burst sparsity to mitigate the noise effect and significantly enhance the overall performance in the low SNR regime, as will be shown in the simulations.

B. Hidden Markov Model for Joint Burst Sparsity

In practice, the radar and communication channels exhibit certain joint burst sparsity as explained in the introduction and illustrated in Fig. 1. In this section, we shall introduce a hidden Markov model to capture the joint burst sparse structure of the radar and communication channels. Specifically, let $\mathbf{s}^r = [s_1^r, \dots, s_M^r]^T$ and $\mathbf{s}^c = [s_1^c, \dots, s_M^c]^T$ denote the support vectors of the radar and communication channels, respectively, where $s_m^r = 1$ ($s_m^c = 1$) indicates there is a radar target (communication scatterer) around the m -th AoA grid θ_m , and $s_m^r = 0$ ($s_m^c = 0$) indicates the opposite. Therefore, in Fig. 1, $\Omega_r \triangleq \{m : s_m^r = 1\}$ indicates the set of (coarse) AoAs of radar targets, $\Omega_c \triangleq \{m : s_m^c = 1\}$ indicates the set of (coarse) AoAs of user, and $\Omega_s \triangleq \Omega_r \cup \Omega_c$ indicates the common AoA set.

Conditioned on the channel support vectors \mathbf{s}^r and \mathbf{s}^c , the elements of \mathbf{x}^r and \mathbf{x}^c are independent and the conditional prior distributions are respectively given by

$$p(x_m^r | s_m^r) = (1 - s_m^r)\delta(x_m^r) + s_m^r \mathcal{CN}(x_m^r; 0, (\sigma_m^r)^2) \quad (7)$$

$$p(x_m^c | s_m^c) = (1 - s_m^c)\delta(x_m^c) + s_m^c \mathcal{CN}(x_m^c; 0, (\sigma_m^c)^2), \quad (8)$$

where $(\sigma_m^r)^2$ and $(\sigma_m^c)^2$ are the variance of x_m^r and x_m^c conditioned on $s_m^r = 1$ and $s_m^c = 1$, respectively.

To represent the common AoAs of the radar and communication channels, a joint support vector $\mathbf{s} = [s_1, \dots, s_M] \in \{0, 1\}^M$ with $s_m = s_m^r \vee s_m^c$ is introduced in the HMM, where \vee represents the logical ‘‘or’’ operator. The joint distribution for the channel support vectors \mathbf{s} , \mathbf{s}^r and \mathbf{s}^c is given by $p(\mathbf{s}, \mathbf{s}^r, \mathbf{s}^c) = p(\mathbf{s})p(\mathbf{s}^r | \mathbf{s})p(\mathbf{s}^c | \mathbf{s})$, where

$$p(\mathbf{s}^r|\mathbf{s}) = \prod_m p(s_m^r|s_m) = \prod_m (1 - s_m)\delta(s_m^r) + s_m\rho_r^{s_m}(1 - \rho_r)^{1-s_m}, \quad (9)$$

$$p(\mathbf{s}^c|\mathbf{s}) = \prod_m p(s_m^c|s_m) = \prod_m (1 - s_m)\delta(s_m^c) + s_m\rho_c^{s_m}(1 - \rho_c)^{1-s_m} \quad (10)$$

where $\rho_r = \frac{|\Omega_r|}{|\Omega_s|}$ ($\rho_c = \frac{|\Omega_c|}{|\Omega_s|}$) is the probability of $s_m^r = 1$ ($s_m^c = 1$) conditioned on $s_m = 1$, which measures the degree of overlapping between the targets and communication scatterers. Furthermore, to capture the burst sparse structure of the joint communication and radar channel, the joint support vector \mathbf{s} is modeled as a Markov chain:

$$p(\mathbf{s}) = p(s_1) \prod_{m=1}^{M-1} p(s_{m+1}|s_m), \quad (11)$$

with the transition probability given by $p(s_{m+1} = 1|s_m = 0) = \rho_{0,1}$ and $p(s_{m+1} = 0|s_m = 1) = \rho_{1,0}$. The initial distribution $p(s_1)$ is set to be the steady state distribution of the Markov chain in (11), i.e.,

$$\lambda \triangleq p(s_m = 1) = \frac{\rho_{0,1}}{\rho_{0,1} + \rho_{1,0}}. \quad (12)$$

The transition probabilities $\rho_{0,1}$ and $\rho_{1,0}$ determine the average length of each non-zero burst and the total number of non-zero bursts in \mathbf{s} , and λ determines the sparsity level of \mathbf{s} .

Finally, the joint prior distribution of all the random variables in HMM is given by

$$p(\mathbf{s}, \mathbf{s}^r, \mathbf{s}^c, \mathbf{x}^r, \mathbf{x}^c) = p(\mathbf{s}) \prod_m p(s_m^r|s_m) \prod_m p(s_m^c|s_m) \prod_m p(x_m^r|s_m^r)p(x_m^c|s_m^c). \quad (13)$$

C. Sparse Bayesian Inference Formulation for Joint Detection and Estimation

The problem formulation and algorithm design for the two stages can be unified by using the same notation $\mathbf{v}_1, \dots, \mathbf{v}_P$ and $\mathbf{y}_1^r, \dots, \mathbf{y}_P^r$ to denote the DPs and the received DP signals in both stages. Specifically, in Stage 1, we have $P = P_1$ and $\mathbf{v}_p = \mathbf{v}_{1,p}$, $\mathbf{y}_p^r = \mathbf{y}_{1,p}^r$, $p = 1, \dots, P_1$. In Stage 2, we have $P = P_1 + P_2$, $\mathbf{v}_p = \mathbf{v}_{1,p}$, $\mathbf{y}_p^r = \mathbf{y}_{1,p}^r$, $p = 1, \dots, P_1$ and $\mathbf{v}_{P_1+p} = \mathbf{v}_{2,p}$, $\mathbf{y}_{P_1+p}^r = \mathbf{y}_{2,p}^r$, $p = 1, \dots, P_2$. For convenience, we define the radar and communication measurement

matrices $\mathbf{F}^r(\boldsymbol{\theta}) \triangleq \mathbf{V}\tilde{\mathbf{A}}(\boldsymbol{\theta}) \in \mathbb{C}^{PM \times M}$ and $\mathbf{F}^c(\boldsymbol{\theta}) \triangleq \mathbf{U}\mathbf{A}(\boldsymbol{\theta}) \in \mathbb{C}^{QM \times M}$, where

$$\mathbf{V} = \begin{bmatrix} \mathbf{v}_1^T \otimes \mathbf{I}_M \\ \dots \\ \mathbf{v}_P^T \otimes \mathbf{I}_M \end{bmatrix}, \quad \mathbf{U} = \begin{bmatrix} u_1 \mathbf{I}_M \\ \dots \\ u_Q \mathbf{I}_M \end{bmatrix},$$

$\tilde{\mathbf{A}}(\boldsymbol{\theta}) \in \mathbb{C}^{M^2 \times M}$ consists of the $(m-1)M + m$ -th column of $\mathbf{A}^*(\boldsymbol{\theta}) \otimes \mathbf{A}(\boldsymbol{\theta})$ for $m = 1, \dots, M$, and \otimes means the Kronecker product. Using these notations, (1) and (3) can be rewritten as a linear observation model as

$$\mathbf{y} = \mathbf{F}(\boldsymbol{\theta})\mathbf{x} + \mathbf{n}, \quad (14)$$

where $\mathbf{y}^c = [(\mathbf{y}^r)^T, (\mathbf{y}^c)^T]^T$, $\mathbf{y}^r = [(\mathbf{y}_1^r)^T, \dots, (\mathbf{y}_P^r)^T]^T$, $\mathbf{x} = [(\mathbf{x}^r)^T, (\mathbf{x}^c)^T]^T$, \mathbf{n} is the aggregated noise vector and $\mathbf{F}(\boldsymbol{\theta}) = \text{BlockDiag}(\mathbf{F}^r(\boldsymbol{\theta}), \mathbf{F}^c(\boldsymbol{\theta}))$.

For given grid parameter $\boldsymbol{\theta}$ and observation \mathbf{y} , we aim at computing the conditional marginal posteriors $p(\mathbf{x}^r | \mathbf{y}, \boldsymbol{\theta})$, $p(\mathbf{x}^c | \mathbf{y}, \boldsymbol{\theta})$, $p(s_m^r | \mathbf{y}, \boldsymbol{\theta})$, $\forall m$ (i.e., perform Bayesian inference for \mathbf{x}^r , \mathbf{x}^c and $s_m^r, s_m^c, \forall m$). On the other hand, the grid parameter is obtained by ML estimation as

$$\boldsymbol{\theta}^* = \underset{\boldsymbol{\theta}}{\text{argmax}} \ln p(\mathbf{y} | \boldsymbol{\theta}). \quad (15)$$

Once we have the ML estimate of $\boldsymbol{\theta}$ and the associated conditional marginal posteriors, the MAP estimate of the communication channel as $\mathbf{x}^{c*} = \underset{\mathbf{x}^c}{\text{argmax}} p(\mathbf{x}^c | \mathbf{y}, \boldsymbol{\theta}^*)$ and $\mathbf{h}^{c*} = \mathbf{A}(\boldsymbol{\theta}^*)\mathbf{x}^{c*}$ can be obtained. Moreover, $p(s_m^r | \mathbf{y}, \boldsymbol{\theta}^*)$ gives the probability that a target exists at the AoA direction θ_m^* .

It is very challenging to calculate the above conditional marginal posteriors because the factor graph of the underlying probability model has loops. In the following subsections, we shall propose a Turbo-SBI algorithm which approximately calculates the marginal posteriors and finds an approximate solution for (15). The proposed Turbo-SBI algorithm is shown in the simulations to achieve a good performance.

D. Outline of the Turbo-SBI Algorithm

Based on the Expectation-maximization (EM) method, the Turbo-SBI algorithm starts from the uniform grid $\boldsymbol{\theta}^0$ and performs iterations between the following two major steps until convergence.

- **Turbo-SBI-E Step:** For given grid parameter θ^i in the i -th iteration, we approximately calculate the posteriors $p(\mathbf{x}^r|\mathbf{y}, \theta^i)$, $p(\mathbf{x}^c|\mathbf{y}, \theta^i)$, $p(s_m^r|\mathbf{y}, \theta^i)$, $\forall m$ by combining the message passing and LMMSE approaches via the turbo framework;
- **Turbo-SBI-M Step:** Using the approximate posterior $p(\mathbf{x}|\mathbf{y}, \theta^i)$ obtained in the Turbo-SBI-E Step, calculate the gradient for the likelihood function $\ln p(\mathbf{y}|\theta)$ at θ^i , then use gradient ascent update to obtain the next iterate θ^{i+1} .

In the following two subsections, we first elaborate how to approximately calculate the posterior $p(\mathbf{x}|\mathbf{y}, \theta^i)$ and the other marginal posteriors $p(s_m^r|\mathbf{y}, \theta^i)$, $\forall m$ in the Turbo-VBI-E Step. Then we present the Turbo-VBI-M Step, which requires the posterior $p(\mathbf{x}|\mathbf{y}, \theta^i)$ calculated in the Turbo-SBI-E step. Note that similar to the grid parameter θ , the parameters $\rho_r, \rho_c, \rho_{0,1}, \rho_{1,0}$ in the HMM prior model can also be automatically learned based on the EM method. Please refer to [30] for the details of the EM method to learn the parameters in the prior model.

E. Turbo-SBI-E Step with Given Grid Parameters

The Turbo-SBI-E Step contains two modules, as shown in Fig. 3. Module A is a LMMSE estimator based on the observation \mathbf{y} and extrinsic messages from Module B. Module B, which is called the HMM-MMSE estimator, performs MMSE estimation that combines the HMM prior and the extrinsic messages from Module A. The two modules are executed iteratively until convergence. In the following, we elaborate the two modules in Fig. 3. Since the grid is fixed in the Turbo-SBI-E Step, we shall omit the grid θ in $\mathbf{F}(\theta)$ in this subsection.

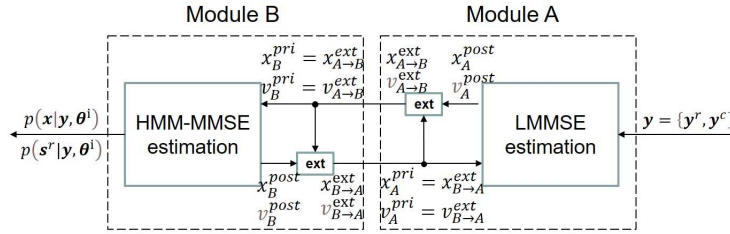


Fig. 3. Modules of the Turbo-SBI-E step and message flow between different modules.

A. *LMMSE in Module A:* In Module A, we assume that \mathbf{x} follows a Gaussian distribution with a prior mean $\mathbf{x}_A^{pri} = \mathbf{x}_{B \rightarrow A}^{ext}$ and covariance $\mathbf{V}_A^{pri} = \mathbf{V}_{B \rightarrow A}^{ext}$, where $\mathbf{x}_{B \rightarrow A}^{ext}$ and $\mathbf{V}_{B \rightarrow A}^{ext}$ are the extrinsic message output from Module B, as will be given in (24). Note that $\mathbf{V}_{B \rightarrow A}^{ext}$ is a diagonal

matrix. With this assumption and the linear observation model $\mathbf{y} = \mathbf{F}\mathbf{x} + \mathbf{n}$, the posterior mean of \mathbf{x} is given by the LMMSE estimator

$$\mathbf{x}_A^{post} = \mathbf{V}_A^{post} \left((\mathbf{V}_A^{pri})^{-1} \mathbf{x}_A^{pri} + \frac{\mathbf{F}^H \mathbf{y}}{\sigma_n^2} \right) \quad (16)$$

and \mathbf{V}_A^{post} is the posterior covariance of \mathbf{x} given by

$$\mathbf{V}_A^{post} = \left(\frac{\mathbf{F}^H \mathbf{F}}{\sigma_n^2} + (\mathbf{V}_A^{pri})^{-1} \right)^{-1}. \quad (17)$$

In the simulations, we note that the off-diagonal elements of $\mathbf{V}_A^{inv} \triangleq \frac{\mathbf{F}^H \mathbf{F}}{\sigma_n^2} + (\mathbf{V}_A^{pri})^{-1}$ are usually much smaller than its diagonal elements, and most non-zero off-diagonal elements concentrate on the five-diagonal sub-matrix of \mathbf{V}_A^{inv} . In fact, for uniform grid $\boldsymbol{\theta}$, \mathbf{V}_A^{inv} reduces to a diagonal matrix. Let $\mathbf{V}_{A,0}^{inv}$ denote the five-diagonal sub-matrix of \mathbf{V}_A^{inv} . By applying the first-order Taylor expansion of $(\mathbf{V}_A^{inv})^{-1}$ at $\mathbf{V}_{A,0}^{inv}$, the calculation of \mathbf{V}_A^{post} can be safely approximated as

$$\mathbf{V}_A^{post} \approx 2\mathbf{V}_{A,0}^{inv} - (\mathbf{V}_{A,0}^{inv})^{-1} \mathbf{V}_A^{inv} (\mathbf{V}_{A,0}^{inv})^{-1}. \quad (18)$$

Then the extrinsic message passed to Module B can be calculated by excluding the prior information $\mathbf{x}_A^{pri}, \mathbf{V}_A^{pri}$ as

$$\begin{aligned} \mathbf{V}_{A \rightarrow B}^{ext} &= \left((\overline{\mathbf{V}}_A^{post})^{-1} - (\mathbf{V}_A^{pri})^{-1} \right)^{-1}, \\ \mathbf{x}_{A \rightarrow B}^{ext} &= \mathbf{V}_{A \rightarrow B}^{ext} \left((\overline{\mathbf{V}}_A^{post})^{-1} \mathbf{x}_A^{post} - (\mathbf{V}_A^{pri})^{-1} \mathbf{x}_A^{pri} \right), \end{aligned} \quad (19)$$

where $\overline{\mathbf{V}}_A^{post}$ is a diagonal approximation of \mathbf{V}_A^{post} by setting the off-diagonal elements to zeros. The above approximations in (18) and $\overline{\mathbf{V}}_A^{post}$ can greatly simplify the calculations with little performance loss, as verified by simulations.

B. Message Passing in Module B: In Module B, a message passing scheme is used for the HMM-MMSE estimator to calculate the posterior of \mathbf{x} and \mathbf{s}^r , based on the HMM channel prior and the extrinsic messages $\mathbf{x}_{A \rightarrow B}^{ext}, \mathbf{V}_{A \rightarrow B}^{ext}$ from Module A. Specifically, the extrinsic messages $\mathbf{x}_{A \rightarrow B}^{ext}, \mathbf{V}_{A \rightarrow B}^{ext}$ are equivalently modeled as a virtual AWGN observation model:

$$\begin{aligned} \mathbf{x}_B^{r,pri} &= \mathbf{x}^r + \mathbf{z}^r, \\ \mathbf{x}_B^{c,pri} &= \mathbf{x}^c + \mathbf{z}^c, \end{aligned}$$

where the extrinsic mean $\mathbf{x}_{A \rightarrow B}^{ext} = [(\mathbf{x}_B^{r,pri})^T, (\mathbf{x}_B^{c,pri})^T]^T$ is treated as observations obtained via a virtual AWGN channel with zero mean noise vectors \mathbf{z}^r and \mathbf{z}^c , and the extrinsic covariance $\mathbf{V}_{A \rightarrow B}^{ext} = \text{BlockDiag}(\mathbf{V}_B^{r,pri}, \mathbf{V}_B^{c,pri})$ is treated as the noise covariance, i.e., $\mathbf{z}^r \sim \mathcal{CN}(0; \mathbf{V}_B^{r,pri})$, $\mathbf{z}^c \sim \mathcal{CN}(0; \mathbf{V}_B^{c,pri})$. Similar treatment has been used in various approximate message passing algorithms, see e.g., [31], [32], [33] for justifications of this treatment. The factor graph \mathcal{G}_B of the joint distribution associated with this virtual AWGN observation model is shown in Fig. 4, where the function expression of each factor node is listed in Table I. In Table I, $x_{B,m}^{r,pri}$ and $x_{B,m}^{c,pri}$ are the m -th elements of $\mathbf{x}_B^{r,pri}$ and $\mathbf{x}_B^{c,pri}$, respectively, and $v_{B,m}^{r,pri}$ and $v_{B,m}^{c,pri}$ are the m -th diagonal elements of $\mathbf{V}_B^{r,pri}$ and $\mathbf{V}_B^{c,pri}$, respectively.

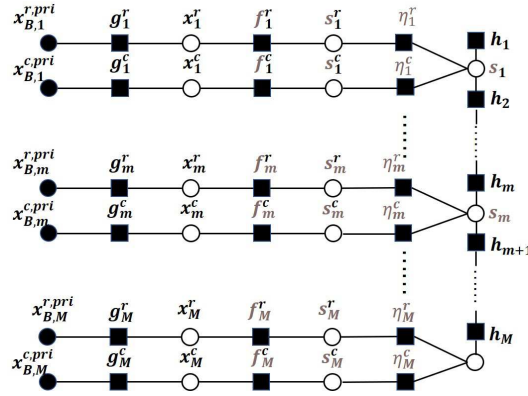


Fig. 4. Factor graph of the joint distribution $p(\mathbf{s}, \mathbf{s}^r, \mathbf{s}^c, \mathbf{x}^r, \mathbf{x}^c, \mathbf{x}_B^{r,pri}, \mathbf{x}_B^{c,pri} | \theta)$.

TABLE I
FACTORS, DISTRIBUTIONS AND FUNCTIONAL FORMS IN FIG. 4.

Factor	Distribution	Functional form
$g_m^r(x_{B,m}^{r,pri}, x_m^r)$	$p(x_m^r x_{B,m}^{r,pri})$	$\mathcal{CN}(x_m^r; x_{B,m}^{r,pri}, v_{B,m}^{r,pri})$
$g_m^c(x_{B,m}^{c,pri}, x_m^c)$	$p(x_m^c x_{B,m}^{c,pri})$	$\mathcal{CN}(x_m^c; x_{B,m}^{c,pri}, v_{B,m}^{c,pri})$
$f_m^r(x_m^r, s_m^r)$	$p(x_m^r s_m^r)$	$(1 - s_m^r) \delta(x_m^r) + s_m^r \mathcal{CN}(x_m^r; 0, (\sigma_m^r)^2)$
$f_m^c(x_m^c, s_m^c)$	$p(x_m^c s_m^c)$	$(1 - s_m^c) \delta(x_m^c) + s_m^c \mathcal{CN}(x_m^c; 0, (\sigma_m^c)^2)$
$\eta_m^r(s_m^r, s_m)$	$p(s_m^r s_m)$	$p(s_m^r = 1 s_m = 0) = 0, p(s_m^r = 1 s_m = 1) = \rho^r$
$\eta_m^c(s_m^c, s_m)$	$p(s_m^c s_m)$	$p(s_m^c = 1 s_m = 0) = 0, p(s_m^c = 1 s_m = 1) = \rho^c$
$h_1^s(s_1)$	$p(s_1)$	$(\lambda)^{s_1} (1 - \lambda)^{1-s_1}$
$h_{m+1}^s(s_{m+1}, s_m)$	$p(s_{m+1} s_m)$	$\begin{cases} (\rho_{0,1})^{s_{m+1}} (1 - \rho_{0,1})^{1-s_{m+1}}, & s_m = 0 \\ (1 - \rho_{1,0})^{s_{m+1}} (\rho_{1,0})^{1-s_{m+1}}, & s_m = 1 \end{cases}$

We now outline the message passing scheme over the factor graph \mathcal{G}_B . The details are

elaborated in Appendix A. According to the sum-product rule, the message passing over $x_m^r \rightarrow f_m^r \rightarrow s_m^r \rightarrow \eta_m^r \rightarrow s_m$ and $x_m^c \rightarrow f_m^c \rightarrow s_m^c \rightarrow \eta_m^c \rightarrow s_m$ are given by (45) - (48). Then a forward backward message passing is performed over the Markov chains \mathbf{s} through (49) - (52). After this, the message is passed back over the path $s_m \rightarrow \eta_m^r \rightarrow s_m^r \rightarrow f_m^r \rightarrow x_m^r$ and $s_m \rightarrow \eta_m^c \rightarrow s_m^c \rightarrow f_m^c \rightarrow x_m^c$ using (53) - (55).

After calculating the updated messages $\{v_{f_m^r \rightarrow x_m^r}\}$, the approximate posterior distributions are given by

$$\hat{p}(x_m^r | \mathbf{y}) \propto v_{f_m^r \rightarrow x_m^r} \times v_{x_m^r \rightarrow f_m^r}, \quad (20)$$

$$\hat{p}(s_m^r | \mathbf{y}) = \frac{\pi_{s^r, m}^{in} \pi_{s^r, m}^{out}}{\pi_{s^r, m}^{in} \pi_{s^r, m}^{out} + (1 - \pi_{s^r, m}^{in})(1 - \pi_{s^r, m}^{out})}, \forall m, \quad (21)$$

where $v_{f_m^r \rightarrow x_m^r}$, $v_{x_m^r \rightarrow f_m^r}$, $\pi_{s^r, m}^{in}$, $\pi_{s^r, m}^{out}$ are given in Appendix A. Then the posterior mean $\mathbf{x}_B^{r, post} = [x_{B,1}^{r, post}, \dots, x_{B,M}^{r, post}]^T$ and variance $\mathbf{V}_B^{r, post} = \text{Diag}([v_{B,1}^{post}, \dots, v_{B,M}^{post}])$ for \mathbf{x}^r can be respectively calculated as

$$x_{B,m}^{r, post} = \int_{x_m^r} x_m^r \hat{p}(x_m^r | \mathbf{y}), \quad (22)$$

$$v_{B,m}^{post} = \int_{x_m^r} |x_m^r - x_{B,m}^{r, post}|^2 \hat{p}(x_m^r | \mathbf{y}), \quad (23)$$

for $m = 1, \dots, M$. The posterior mean $\mathbf{x}_B^{c, post}$ and variance $\mathbf{V}_B^{c, post}$ for \mathbf{x}^c can be calculated similarly. Then the extrinsic message passed to Module A can be calculated as

$$\begin{aligned} \mathbf{V}_{B \rightarrow A}^{ext} &= ((\mathbf{V}_B^{post})^{-1} - (\mathbf{V}_B^{pri})^{-1})^{-1}, \\ \mathbf{x}_{B \rightarrow A}^{ext} &= \mathbf{V}_{B \rightarrow A}^{ext} ((\mathbf{V}_B^{post})^{-1} \mathbf{x}_B^{post} - (\mathbf{V}_B^{pri})^{-1} \mathbf{x}_B^{pri}), \end{aligned} \quad (24)$$

where $\mathbf{x}_B^{pri} = [(\mathbf{x}_B^{r, pri})^T, (\mathbf{x}_B^{c, pri})^T]^T$, $\mathbf{x}_B^{post} = [(\mathbf{x}_B^{r, post})^T, (\mathbf{x}_B^{c, post})^T]^T$, $\mathbf{V}_B^{pri} \triangleq \text{BlockDiag}(\mathbf{V}_B^{r, pri}, \mathbf{V}_B^{c, pri})$ and $\mathbf{V}_B^{post} \triangleq \text{BlockDiag}(\mathbf{V}_B^{r, post}, \mathbf{V}_B^{c, post})$.

Finally, we point out that the Turbo-OAMP in [27] is an approximation of the proposed Turbo-SBI-E Step when \mathbf{F} is PO. Specifically, in Turbo-OAMP, by assuming a PO measurement matrix \mathbf{F} , the $\mathbf{F}^H \mathbf{F}$ in the LMMSE Step in (17) is approximated as $\mathbf{F}^H \mathbf{F} \approx \frac{\text{tr}(\mathbf{F}^H \mathbf{F})}{2M} \mathbf{I}$. Moreover, when calculating the extrinsic messages in (19) and (24), \mathbf{V}_B^{post} and \mathbf{V}_B^{post} are approximated as $v_A^{post} \mathbf{I}$ and $v_B^{post} \mathbf{I}$, respectively, where v_A^{post} and v_B^{post} are the mean values of the diagonal elements of \mathbf{V}_B^{post} and \mathbf{V}_B^{post} , respectively.

F. Turbo-SBI-M Step

In the M step, we need to maximize the log-likelihood function $\ln p(\mathbf{y}|\boldsymbol{\theta})$, which is difficult because $\ln p(\mathbf{y}|\boldsymbol{\theta})$ does not have a closed-form expression. Inspired by the EM method, we construct a surrogate function for $\ln p(\mathbf{y}|\boldsymbol{\theta})$ around the current iterate $\boldsymbol{\theta}^i$ as follows

$$\begin{aligned} Q(\boldsymbol{\theta}; \boldsymbol{\theta}^i) &= \int p(\mathbf{x}|\mathbf{y}, \boldsymbol{\theta}^i) \ln \frac{p(\mathbf{y}, \mathbf{x}|\boldsymbol{\theta})}{p(\mathbf{x}|\mathbf{y}, \boldsymbol{\theta}^i)} d\mathbf{x} \\ &= -\frac{\|\mathbf{y} - \mathbf{F}(\boldsymbol{\theta})\mathbf{x}^{post}\|_2^2 + \text{tr}(\mathbf{F}(\boldsymbol{\theta})\mathbf{V}^{post}\mathbf{F}(\boldsymbol{\theta})^H)}{\sigma_n^2} + c, \end{aligned}$$

where \mathbf{x}^{post} and \mathbf{V}^{post} denote the posterior mean and covariance associated with $p(\mathbf{x}|\mathbf{y}, \boldsymbol{\theta}^i)$, and c is a constant. It can be shown that $Q(\boldsymbol{\theta}; \boldsymbol{\theta}^i) \leq \ln p(\mathbf{y}|\boldsymbol{\theta})$, $\forall \boldsymbol{\theta}$, $Q(\boldsymbol{\theta}^i; \boldsymbol{\theta}^i) = \ln p(\mathbf{y}|\boldsymbol{\theta}^i)$ and $\nabla_{\boldsymbol{\theta}} Q(\boldsymbol{\theta}^i; \boldsymbol{\theta}^i) = \nabla_{\boldsymbol{\theta}} \ln p(\mathbf{y}|\boldsymbol{\theta}^i)$. Based on this, the next iterate $\boldsymbol{\theta}^{i+1}$ can be obtained using the gradient ascent method as

$$\boldsymbol{\theta}^{i+1} = \boldsymbol{\theta}^i + \tau^i \nabla_{\boldsymbol{\theta}} Q(\boldsymbol{\theta}^i; \boldsymbol{\theta}^i), \quad (25)$$

where τ^i is the step size which can be determined by applying the Arjimo rule to $Q(\boldsymbol{\theta}; \boldsymbol{\theta}^i)$. The Arjimo rule ensures that $Q(\boldsymbol{\theta}^{i+1}; \boldsymbol{\theta}^i) \geq Q(\boldsymbol{\theta}^i; \boldsymbol{\theta}^i)$ and the equality only holds when $\boldsymbol{\theta}^i$ is already a stationary point of the ML estimation problem. Therefore, we have $\ln p(\mathbf{y}|\boldsymbol{\theta}^{i+1}) \geq Q(\boldsymbol{\theta}^{i+1}; \boldsymbol{\theta}^i) \geq Q(\boldsymbol{\theta}^i; \boldsymbol{\theta}^i) = \ln p(\mathbf{y}|\boldsymbol{\theta}^i)$, i.e., the Turbo-SBI-M Step can strictly increase the likelihood function until convergence to a stationary point. Finally, the gradient $\nabla_{\boldsymbol{\theta}} Q(\boldsymbol{\theta}^i; \boldsymbol{\theta}^i) = \left[\frac{\partial Q(\boldsymbol{\theta}^i; \boldsymbol{\theta}^i)}{\partial \theta_1}, \dots, \frac{\partial Q(\boldsymbol{\theta}^i; \boldsymbol{\theta}^i)}{\partial \theta_M} \right]^T$ is given by

$$\begin{aligned} \frac{\partial Q(\boldsymbol{\theta}^i; \boldsymbol{\theta}^i)}{\partial \theta_m} &= 2\text{Re}[\mathbf{a}'(\theta_m^i)^H \mathbf{U}^H \mathbf{U} \mathbf{a}(\theta_m^i) \mathbf{c}_1^i + \mathbf{a}'(\theta_m^i)^H \mathbf{U}^H \mathbf{c}_2^i] \\ &\quad + 2\text{Re}[\tilde{\mathbf{a}}'(\theta_m^i)^H \mathbf{V}^H \mathbf{V} \tilde{\mathbf{a}}(\theta_m^i) \mathbf{c}_3^i + \tilde{\mathbf{a}}'(\theta_m^i)^H \mathbf{V}^H \mathbf{c}_4^i], \end{aligned} \quad (26)$$

where $\tilde{\mathbf{a}}(\theta_m^i)$ is the m -th column of $\tilde{\mathbf{A}}(\boldsymbol{\theta})$, $\mathbf{y}_{-m}^{c,i} = \mathbf{y}^c - \mathbf{U} \sum_{j \neq m} (x_{A,j}^{c,post} \cdot \mathbf{a}(\theta_j^i))$,

$$\mathbf{y}_{-m}^{r,i} = \mathbf{y}^r - \mathbf{V} \sum_{j \neq m} (x_{A,j}^{r,post} \cdot \tilde{\mathbf{a}}(\theta_j^i)), \quad \mathbf{a}'(\theta_m^i) = d\mathbf{a}(\boldsymbol{\theta}^i)/d\theta_m^i, \quad \tilde{\mathbf{a}}'(\theta_m^i) = d\tilde{\mathbf{a}}_m(\boldsymbol{\theta}^i)/d\theta_m^i,$$

$$\begin{aligned} \mathbf{c}_1^i &= -\sigma_n^{-2} \left(|x_{A,m}^{c,post}|^2 + v_{A,m}^{c,post} \right), \quad \mathbf{c}_2^i = \sigma_n^{-2} \left((x_{A,m}^{c,post})^* \mathbf{y}_{-m}^{c,i} - \mathbf{U} \sum_{j \neq m} v_{A,j}^{c,post} \mathbf{a}(\theta_j^i) \right), \\ \mathbf{c}_3^i &= -\sigma_n^{-2} \left(|x_{A,m}^{r,post}|^2 + v_{A,m}^{r,post} \right), \quad \mathbf{c}_4^i = \sigma_n^{-2} \left((x_{A,m}^{r,post})^* \mathbf{y}_{-m}^{r,i} - \mathbf{V} \sum_{j \neq m} v_{A,j}^{r,post} \tilde{\mathbf{a}}(\theta_j^i) \right). \end{aligned}$$

Note that to calculate $Q(\boldsymbol{\theta}; \boldsymbol{\theta}^i)$ and its gradient, we need to know the posterior mean and covariance \mathbf{x}^{post} and \mathbf{V}^{post} associated with $p(\mathbf{x}|\mathbf{y}, \boldsymbol{\theta}^i)$, which can be approximated using the

\mathbf{x}_B^{post} and \mathbf{V}_B^{post} calculated in the Turbo-SBI-E Step. Finally, the overall Turbo-SBI algorithm is summarized in Algorithm 1.

Algorithm 1 Turbo-SBI algorithm

Input: \mathbf{y} , $\boldsymbol{\theta}^0$, maximum iteration numbers I_{in} , I_{out} , threshold ϵ .

Output: $\boldsymbol{\theta}^*$, \mathbf{x}^* , $\hat{p}(s_m^r | \mathbf{y}, \boldsymbol{\theta}^*)$, $\forall m$.

for $i = 1, \dots, I_{out}$ **do**

Turbo-SBI-E Step:

 Initialize $i_{in} = 1$, $\mathbf{x}_A^{pri} = \mathbf{0}$ and \mathbf{V}_A^{pri} .

while not converge and $i_{in} \leq I_{in}$ **do**

$i_{in} = i_{in} + 1$.

%Module A: LMMSE Estimator

 Update \mathbf{x}_A^{post} and \mathbf{V}_A^{post} , using (16) and (17)/(18).

 Update $\mathbf{x}_B^{pri} = \mathbf{x}_{A \rightarrow B}^{ext}$ and $\mathbf{V}_B^{pri} = \mathbf{V}_{A \rightarrow B}^{ext}$, using (19).

%Module B: HMM-MMSE Estimator

 Perform message passing over the factor graph \mathcal{G}_B using (45) - (55).

 Calculate the approximate posterior distributions $\hat{p}(x_m^r | \mathbf{y}, \boldsymbol{\theta}^i)$, $\hat{p}(s_m^r | \mathbf{y}, \boldsymbol{\theta}^i)$, $\forall m$ using (20), (21).

 Update \mathbf{x}_B^{post} and \mathbf{V}_B^{post} using (22) and (23).

 Update $\mathbf{x}_A^{pri} = \mathbf{x}_{B \rightarrow A}^{ext}$ and $\mathbf{V}_A^{pri} = \mathbf{V}_{B \rightarrow A}^{ext}$, using (24).

end while

Turbo-SBI-M Step:

 Calculate the gradient $\frac{\partial Q(\boldsymbol{\theta}^i; \boldsymbol{\theta}^i)}{\partial \theta_m}$ in (26) using the \mathbf{x}_B^{post} and \mathbf{V}_B^{post} from the E step.

 Obtain $\boldsymbol{\theta}^{i+1}$ using the gradient ascent update in (25).

if $\|\boldsymbol{\theta}^{i+1} - \boldsymbol{\theta}^i\| \leq \epsilon$ **then**

break

end if

end for

Output $\boldsymbol{\theta}^*$, $\mathbf{x}^* = \mathbf{x}_B^{post}$ and $\hat{p}(s_m^r | \mathbf{y}, \boldsymbol{\theta}^*)$.

G. Complexity Analysis of Turbo-SBI

The complexity of Module A is mainly dominated by the matrix inverse operation in (17), whose complexity is $O(M^3)$. By using the first-order Taylor expansion in (18), we can reduce the complexity of Module A to $O(M^2)$. The complexity of Module B is $O(M)$ since it only involves scalar or diagonal matrix operations. Finally, the complexity of the gradient ascent update for the off-grid parameter in (25) is dominated by the matrix multiplication $\mathbf{V}\tilde{\mathbf{a}}(\theta_m^i)$, whose complexity is $O(M^2P)$. Therefore, the overall per outer iteration complexity of the Turbo-SBI is $O(I_{in}M^2 + M^2P)$.

IV. OPTIMAL PILOT DESIGN BASED ON CRAMER-RAO BOUND

In this section, we present the pilot design based on the estimated AoAs in Stage 1. We first derive the Cramer-Rao Bound (CRB) of the AoAs. Then we formulate the pilot optimization problem as a worst-case CRB minimization problem. Finally, we propose an efficient algorithm to solve the pilot optimization problem.

A. Derivation of Cramer-Rao Bound

In this subsection, we derive the CRB of the AoAs under the assumption of known channel coefficients x_k^r 's and x_l^c 's. The unknown AoA parameters $\boldsymbol{\theta} = \left[(\boldsymbol{\theta}^r)^T, (\boldsymbol{\theta}^s)^T, (\boldsymbol{\theta}^c)^T \right]^T$ are divided into three subsets, namely, the AoAs of the purely radar targets $\boldsymbol{\theta}^r$, the AoAs of the purely communication paths $\boldsymbol{\theta}^c$, and the common AoAs $\boldsymbol{\theta}^s$. Note that, we use $\boldsymbol{\theta}$ to denote the set of all AoA parameters in this section, even though $\boldsymbol{\theta}$ has been used to denote the dynamic grid in Section III. As in [34], the Fisher Information Matrix (FIM) $\mathbf{J}(\boldsymbol{\theta})$ is defined by

$$\mathbf{J}(\boldsymbol{\theta}) = \mathbb{E} \left\{ \left[\frac{\partial \ln p(\mathbf{y} | \boldsymbol{\theta})}{\partial \boldsymbol{\theta}} \right] \left[\frac{\partial \ln p(\mathbf{y} | \boldsymbol{\theta})}{\partial \boldsymbol{\theta}} \right]^T \right\}, \quad (27)$$

where $p(\mathbf{y} | \boldsymbol{\theta})$ is the likelihood function of the observation \mathbf{y} and $\frac{\partial \ln p(\mathbf{y} | \boldsymbol{\theta})}{\partial \boldsymbol{\theta}}$ is the gradient vector of the log-likelihood function with respect to $\boldsymbol{\theta}$. According to this definition, the FIM based on the reflected DP signals and received UP signals is given by

$$\mathbf{J}(\boldsymbol{\theta}) = \begin{bmatrix} \mathbf{J}(\boldsymbol{\theta}^r, \boldsymbol{\theta}^r) & \mathbf{J}(\boldsymbol{\theta}^r, \boldsymbol{\theta}^s) & \mathbf{J}(\boldsymbol{\theta}^r, \boldsymbol{\theta}^c) \\ \mathbf{J}(\boldsymbol{\theta}^r, \boldsymbol{\theta}^s)^T & \mathbf{J}(\boldsymbol{\theta}^s, \boldsymbol{\theta}^s) & \mathbf{J}(\boldsymbol{\theta}^s, \boldsymbol{\theta}^c) \\ \mathbf{J}(\boldsymbol{\theta}^r, \boldsymbol{\theta}^c)^T & \mathbf{J}(\boldsymbol{\theta}^s, \boldsymbol{\theta}^c)^T & \mathbf{J}(\boldsymbol{\theta}^c, \boldsymbol{\theta}^c) \end{bmatrix}, \quad (28)$$

and the submatrices in $\mathbf{J}(\boldsymbol{\theta})$ are given by

$$\mathbf{J}(\boldsymbol{\theta}^r, \boldsymbol{\theta}^c) = \mathbf{0}, \mathbf{J}(\boldsymbol{\theta}^c, \boldsymbol{\theta}^c) = 2(\sigma_n^c)^{-2} \operatorname{Re} \left\{ \frac{\partial \mathbf{h}^c}{\partial \boldsymbol{\theta}^c} (\boldsymbol{\Psi}^c)^T (\boldsymbol{\Psi}^c)^* \left(\frac{\partial \mathbf{h}^c}{\partial \boldsymbol{\theta}^c} \right)^H \right\} \quad (29)$$

$$\mathbf{J}(\boldsymbol{\theta}^r, \boldsymbol{\theta}^r) = 2(\sigma_n^r)^{-2} \operatorname{Re} \left\{ \frac{\partial \mathbf{h}^r}{\partial \boldsymbol{\theta}^r} (\boldsymbol{\Psi}_1^r)^T (\boldsymbol{\Psi}_1^r)^* \left(\frac{\partial \mathbf{h}^r}{\partial \boldsymbol{\theta}^r} \right)^H \right\} + 2(\sigma_n^r)^{-2} \operatorname{Re} \left\{ \frac{\partial \mathbf{h}^r}{\partial \boldsymbol{\theta}^r} (\boldsymbol{\Psi}_2^r)^T (\boldsymbol{\Psi}_2^r)^* \left(\frac{\partial \mathbf{h}^r}{\partial \boldsymbol{\theta}^r} \right)^H \right\}, \quad (30)$$

$$\mathbf{J}(\boldsymbol{\theta}^r, \boldsymbol{\theta}^s) = 2(\sigma_n^r)^{-2} \operatorname{Re} \left\{ \frac{\partial \mathbf{h}^r}{\partial \boldsymbol{\theta}^r} (\boldsymbol{\Psi}_1^r)^T (\boldsymbol{\Psi}_1^r)^* \left(\frac{\partial \mathbf{h}^r}{\partial \boldsymbol{\theta}^s} \right)^H \right\} + 2(\sigma_n^r)^{-2} \operatorname{Re} \left\{ \frac{\partial \mathbf{h}^r}{\partial \boldsymbol{\theta}^r} (\boldsymbol{\Psi}_2^r)^T (\boldsymbol{\Psi}_2^r)^* \left(\frac{\partial \mathbf{h}^r}{\partial \boldsymbol{\theta}^s} \right)^H \right\}, \quad (31)$$

$$\begin{aligned} \mathbf{J}(\boldsymbol{\theta}^s, \boldsymbol{\theta}^s) &= 2(\sigma_n^r)^{-2} \operatorname{Re} \left\{ \frac{\partial \mathbf{h}^r}{\partial \boldsymbol{\theta}^s} (\boldsymbol{\Psi}_1^r)^T (\boldsymbol{\Psi}_1^r)^* \left(\frac{\partial \mathbf{h}^r}{\partial \boldsymbol{\theta}^s} \right)^H \right\} + 2(\sigma_n^r)^{-2} \operatorname{Re} \left\{ \frac{\partial \mathbf{h}^r}{\partial \boldsymbol{\theta}^s} (\boldsymbol{\Psi}_2^r)^T (\boldsymbol{\Psi}_2^r)^* \left(\frac{\partial \mathbf{h}^r}{\partial \boldsymbol{\theta}^s} \right)^H \right\} \\ &+ 2(\sigma_n^c)^{-2} \operatorname{Re} \left\{ \frac{\partial \mathbf{h}^c}{\partial \boldsymbol{\theta}^s} (\boldsymbol{\Psi}^c)^T (\boldsymbol{\Psi}^c)^* \left(\frac{\partial \mathbf{h}^c}{\partial \boldsymbol{\theta}^s} \right)^H \right\}, \end{aligned} \quad (32)$$

$$\mathbf{J}(\boldsymbol{\theta}^c, \boldsymbol{\theta}^s) = 2(\sigma_n^c)^{-2} \operatorname{Re} \left\{ \frac{\partial \mathbf{h}^c}{\partial \boldsymbol{\theta}^c} (\boldsymbol{\Psi}^c)^T (\boldsymbol{\Psi}^c)^* \left(\frac{\partial \mathbf{h}^c}{\partial \boldsymbol{\theta}^s} \right)^H \right\}. \quad (33)$$

where $\mathbf{h}^r \triangleq \operatorname{vec} \left[(\mathbf{H}^r)^T \right]$ and the aggregated pilot matrices $\boldsymbol{\Psi}_1^r, \boldsymbol{\Psi}_2^r$ and $\boldsymbol{\Psi}^c$ are given by

$$\boldsymbol{\Psi}_1^r = \begin{bmatrix} \mathbf{I}_M \otimes \mathbf{v}_{1,1}^T \\ \dots \\ \mathbf{I}_M \otimes \mathbf{v}_{1,P_1}^T \end{bmatrix}, \quad \boldsymbol{\Psi}_2^r = \begin{bmatrix} \mathbf{I}_M \otimes \mathbf{v}_{2,1}^T \\ \dots \\ \mathbf{I}_M \otimes \mathbf{v}_{2,P_2}^T \end{bmatrix}, \quad \boldsymbol{\Psi}^c = \begin{bmatrix} u_{1,1} \mathbf{I}_M \\ \dots \\ u_{1,Q} \mathbf{I}_M \end{bmatrix} \quad (34)$$

In this section, we shall optimize the radar pilot (DP) in Stage 2 to refine the estimation performance of the AoAs $\boldsymbol{\theta}^r, \boldsymbol{\theta}^s$ for radar targets. The Cramer-Rao (CR) matrix for $\boldsymbol{\theta}^r, \boldsymbol{\theta}^s$ is given by

$$\mathbf{CRB} \triangleq \mathbf{J}_{\text{eff}}^{-1}, \quad (35)$$

where \mathbf{J}_{eff} denotes the Equivalent Fisher Information Matrix (EFIM) of radar targets given by (36). The diagonal elements of the CR matrix provide a lower bound for the MSE of any unbiased estimator of $\boldsymbol{\theta}^r, \boldsymbol{\theta}^s$.

$$\mathbf{J}_{\text{eff}} = \begin{bmatrix} \mathbf{J}(\boldsymbol{\theta}^r, \boldsymbol{\theta}^r) & \mathbf{J}(\boldsymbol{\theta}^r, \boldsymbol{\theta}^s) \\ \mathbf{J}(\boldsymbol{\theta}^r, \boldsymbol{\theta}^s)^T & \mathbf{J}(\boldsymbol{\theta}^s, \boldsymbol{\theta}^s) - \mathbf{J}(\boldsymbol{\theta}^s, \boldsymbol{\theta}^c) \mathbf{J}^{-1}(\boldsymbol{\theta}^c, \boldsymbol{\theta}^c) \mathbf{J}^T(\boldsymbol{\theta}^s, \boldsymbol{\theta}^c) \end{bmatrix} \quad (36)$$

B. Problem Formulation for Pilot Design

There are three commonly used criteria involving a scalar measure of the CR matrix [26]. The first criterion is associated with the minimization of the log-determinant of the CR matrix corresponding to the minimization of the volume of the confidence ellipsoid. The second criterion is the minimization of the trace of the CR matrix, which is associated with the sum of squared errors. The third criterion is the minimization of the maximal eigenvalue, λ_{\max} , of the CR matrix. This criterion is associated with minimizing the worst-case (largest) squared error. In practice, the desired pilot must guarantee the sensing performance of the worst target. Therefore, we adopt the third criterion in this paper.

Since the minimization of the maximal eigenvalue, $\lambda_{\max}^{\text{CR}}$, of the CR matrix is equivalent to maximizing of the minimal eigenvalue, $\lambda_{\min}^{\text{EFIM}}$, of the EFIM \mathbf{J}_{eff} , the optimization problem for DP (radar pilot) design can be formulated as

$$\begin{aligned} \mathcal{P} : \quad & \max_{\{\mathbf{v}_{2,p}\}_{p=1}^{P_2}} \lambda \\ \text{s.t.} \quad & \text{tr}(\mathbf{v}_{2,p}\mathbf{v}_{2,p}^H) \leq P_t, \\ & \mathbf{J}_{\text{eff}}\left(\{\mathbf{v}_{2,p}\}_{p=1}^{P_2}\right) \succeq \lambda\mathbf{I}, \end{aligned} \quad (37)$$

where P_t is the transmit power for target detection, and we have explicitly written \mathbf{J}_{eff} as a function of the optimization variables. Note that the constraint $\mathbf{J}_{\text{eff}}\left(\{\mathbf{v}_{2,p}\}_{p=1}^{P_2}\right) \succeq \lambda\mathbf{I}$ ensures that $\lambda_{\min}^{\text{EFIM}} \geq \lambda$. Therefore, Problem \mathcal{P} maximizes the minimal eigenvalue $\lambda_{\min}^{\text{EFIM}}$ of the EFIM \mathbf{J}_{eff} .

C. Pilot Optimization Algorithm

Notice that Problem \mathcal{P} is not a convex optimization problem since the constraint $\mathbf{J}_{\text{eff}}\left(\{\mathbf{v}_{2,p}\}_{p=1}^{P_2}\right) \succeq \lambda\mathbf{I}$ is not convex w.r.t $\{\mathbf{v}_{2,p}\}_{p=1}^{P_2}$. It can be observed that each submatrix of the FIM can be rewritten as a function of $\{\mathbf{V}_{2,p} \triangleq \mathbf{v}_{2,p}\mathbf{v}_{2,p}^H\}_{p=1}^{P_2}$ as follows,

$$\begin{aligned} \mathbf{J}(\boldsymbol{\theta}^r, \boldsymbol{\theta}^r) &= 2(\sigma_n^r)^{-2} \text{Re} \left\{ \frac{\partial \mathbf{h}^r}{\partial \boldsymbol{\theta}^r} (\boldsymbol{\Psi}_2^r)^T (\boldsymbol{\Psi}_2^r)^* \left(\frac{\partial \mathbf{h}^r}{\partial \boldsymbol{\theta}^r} \right)^H \right\} + \text{constant} \\ &= 2(\sigma_n^r)^{-2} \text{Re} \left\{ \frac{\partial \mathbf{h}^r}{\partial \boldsymbol{\theta}^r} \text{BlockDiag} \left(\sum_p \mathbf{V}_{2,p}, \dots, \sum_p \mathbf{V}_{2,p} \right) \left(\frac{\partial \mathbf{h}^r}{\partial \boldsymbol{\theta}^r} \right)^H \right\} + \text{constant}. \end{aligned} \quad (38)$$

Motivated by the above observation, we convert the original problem into a semi-definite programming with rank-1 constraints by introducing new variables $\{\mathbf{V}_{2,p} = \mathbf{v}_{2,p}\mathbf{v}_{2,p}^H\}_{p=1}^{P_2}$. The optimization problem can then be equivalently reformulated as

$$\begin{aligned} \mathcal{P}_1 : \max_{\{\mathbf{V}_{2,p}\}_{p=1}^{P_2}} \lambda \\ \text{s.t. } \text{tr}(\mathbf{V}_{2,p}) \leq P_t, \end{aligned} \quad (39)$$

$$\mathbf{J}_{\text{eff}}\left(\{\mathbf{V}_{2,p}\}_{p=1}^{P_2}\right) \succeq \lambda \mathbf{I}, \quad (40)$$

$$\text{rank}(\mathbf{V}_{2,p}) = 1, p = 1, 2, \dots, P_2.$$

It can be shown that $\mathbf{J}_{\text{eff}}\left(\{\mathbf{V}_{2,p}\}_{p=1}^{P_2}\right) \succeq \lambda \mathbf{I}$ is a convex constraint. However, the rank-1 constraints $\text{rank}(\mathbf{V}_{2,p}) = 1, p = 1, 2, \dots, P_2$ are still non-convex. To overcome this challenge, we propose to replace the rank-1 constraint with a tight and smooth approximation as stated in the following lemma.

Lemma 1. *The rank of a positive semi-definite matrix $\mathbf{V} \in \mathbb{C}^{M \times M}$ satisfies*

$$\text{rank}(\mathbf{V}) = \lim_{\varepsilon \rightarrow 0} \frac{M \log\left(\frac{1}{\varepsilon}\right) + \log|\mathbf{V} + \varepsilon \mathbf{I}|}{\log\left(1 + \frac{1}{\varepsilon}\right)}. \quad (41)$$

Moreover, for any given $\varepsilon > 0$, the RHS of (41) is a concave function of \mathbf{V} .

Proof: Please refer to Appendix B for the proof. ■

Using Lemma 1, \mathcal{P}_1 can be well approximated by the following problem for small ε

$$\begin{aligned} \mathcal{P}_\varepsilon : \max_{\{\mathbf{V}_{2,p}\}_{p=1}^{P_2}} \lambda \\ \text{s.t. (39) and (40),} \\ M \log\left(\frac{1}{\varepsilon}\right) + \log|\mathbf{V}_{2,p} + \varepsilon \mathbf{I}| \leq \log\left(1 + \frac{1}{\varepsilon}\right), \forall p. \end{aligned} \quad (42)$$

In fact, it can be shown that the optimal solution of \mathcal{P}_ε converges to that of \mathcal{P}_1 as $\varepsilon \rightarrow 0$. Since $M \log\left(\frac{1}{\varepsilon}\right) + \log|\mathbf{V}_{2,p} + \varepsilon \mathbf{I}|$ is concave, we can apply the MM method to find a stationary point of \mathcal{P}_1 . Specifically, the MM method starts from an initial point $\{\mathbf{V}_{2,p}^0\}_{p=1}^{P_2}$, and in the i -th iteration, it solves a locally convex approximation of \mathcal{P}_1 around $\{\mathbf{V}_{2,p}^{i-1}\}_{p=1}^{P_2}$ to obtain the next

iterate $\{\mathbf{V}_{2,p}^i\}_{p=1}^{P_2}$ as:

$$\begin{aligned} \mathcal{P}_c : \max_{\{\mathbf{V}_{2,p}\}_{p=1}^{P_2}} \lambda \\ \text{s.t. (39) and (40),} \end{aligned} \quad (43)$$

$$\begin{aligned} & \text{tr} \left\{ [\mathbf{V}_{2,p}^{i-1} + \varepsilon \mathbf{I}]^{-1} [\mathbf{V}_{2,p} - \mathbf{V}_{2,p}^{i-1}] \right\} \\ & \leq \log \left(1 + \frac{1}{\varepsilon} \right) - M \log \left(\frac{1}{\varepsilon} \right) - \log |\mathbf{V}_{2,p}^{i-1} + \varepsilon \mathbf{I}|, \forall p, \end{aligned} \quad (44)$$

where (43) is obtained by the first-order Taylor expansion of the constraint function in (42).

The overall algorithm is summarized as in Algorithm 2. To ensure the rank-1 constraints are strictly satisfied, a rank-1 projection is adopted in the final step as $\mathbf{v}_{2,p}^* = \tilde{\mathbf{V}}_{2,p}^*(:, 1)$, where $\tilde{\mathbf{V}}_{2,p}^*(:, 1)$ is the dominant eigenvector of $\mathbf{V}_{2,p}^*$. Note that since the constraint function in (42) is a very good approximation of the rank-1 constraint, $\mathbf{V}_{2,p}^*$ will be close to a rank-1 matrix and thus the performance loss caused by the rank-1 projection is tiny. Algorithm 2 requires the knowledge of AoAs $\boldsymbol{\theta}$ and radar/communication channels $\mathbf{h}^c, \mathbf{h}^r$, whose estimated values can be obtained using the Turbo-SBI algorithm in Stage 1. In the simulations, we show that the performance loss caused by using the estimated values of $\boldsymbol{\theta}$ and $\mathbf{h}^c, \mathbf{h}^r$ in Stage 1 is acceptable.

Algorithm 2 The Pilot Optimization Algorithm

Input: P_t , a feasible $\mathbf{V}_{2,p}^0$, maximum iteration numbers I_{max} , threshold ϵ .

Output: $\mathbf{v}_{2,p}^*, \forall p$.

for $i = 1, \dots, I_{max}$ **do**

Obtain the next iterate $(\mathbf{V}_{2,p})^i$ by solving the locally convex approximation problem \mathcal{P}_c .

if $\left\| \mathbf{J}_{\text{eff}} \left(\{\mathbf{V}_{2,p}^i\}_{p=1}^{P_2} \right) - \mathbf{J}_{\text{eff}} \left(\{\mathbf{V}_{2,p}^{i-1}\}_{p=1}^{P_2} \right) \right\| \leq \epsilon$ **then**

break

end if

end for

Let $\mathbf{v}_{2,p}^* = \tilde{\mathbf{V}}_{2,p}^*(:, 1), \forall p$ and output $\mathbf{V}_{2,p}^*, \forall p$.

V. SIMULATION RESULTS

In this section, we shall use simulations under the CDL channel model in 3GPP R15 [28] to verify that the proposed J-PoTdCe scheme can achieve superior performance over the following baseline schemes/algorithms.

- **Separate design using ML-based two-step detection and estimation (SD-MLTS) [17]:** The target detection and channel estimation are performed separately using the ML-based two-step detection and estimation algorithm in [17] with omnidirectional pilots.
- **Separate design using Turbo-SBI (SD-SBI):** The target detection and channel estimation are performed separately using the proposed Turbo-SBI algorithm (i.e., assuming independent sparse channel priors for communication and radar sensing), with omnidirectional pilots.
- **Joint design with random pilots (JDRP):** The target detection and channel estimation are performed jointly using the proposed Turbo-SBI algorithm with omnidirectional pilots.
- **Joint design with SDR-based pilots (JDSDR):** The target detection and channel estimation are performed jointly using the proposed Turbo-SBI algorithm with the pilots optimized using the SDR method.
- **Genie-aided J-PoTdCe:** This is the proposed scheme with the pilots optimized based on the genie-aided information, i.e., the true values of AoAs θ and channels $\mathbf{h}^c, \mathbf{h}^r$.

In the simulation, the BS is equipped with a ULA of $M = 64$ antennas. We set $P_1 = P_2 = 1$. For convenience, define the common sparsity ratio as $\rho_c = |\Omega_r \cap \Omega_c| / \Omega_s$. When $\rho_c = 1$, the radar and communication channels share the same common AoA set Ω_s . Therefore, ρ_c reflects the correlation among the AoA sets of the two channels. To control the common sparsity ratio ρ_c in the simulations, we first generate the communication channel according to the CDL model. Then we randomly choose a proper number of the AoAs of the communication channel as part of the AoAs of the radar channel and the other AoAs of the radar channel are generated similar to the CDL model. The received SNR is set as 3dB. For estimation performance, we compare the average and worst-case MSE of the target AoA and the normalized MSE (NMSE) of the communication and radar channels. We also compare the target detection performance in terms of both false alarm probability and miss detection probability. Specifically, for SD-MLTS, the target detection method is given in (20) in [17]. For all other algorithms, the BS claims a target is detected around the m -th AoA direction if $p^{post}(s_m^r = 1) > 0.5$, where $p^{post}(s_m^r = 1)$ is the posterior probability of $s_m^r = 1$ obtained by the detection algorithm.

A. Convergence Performance of Pilot Optimization Algorithm

Fig. 5 illustrates the convergence of the MM-based pilot optimization algorithm. As can be observed, the proposed pilot optimization algorithm converges quickly within about 5 iterations, and the achieved objective value is better than that of the SDR-based pilot optimization algorithm.

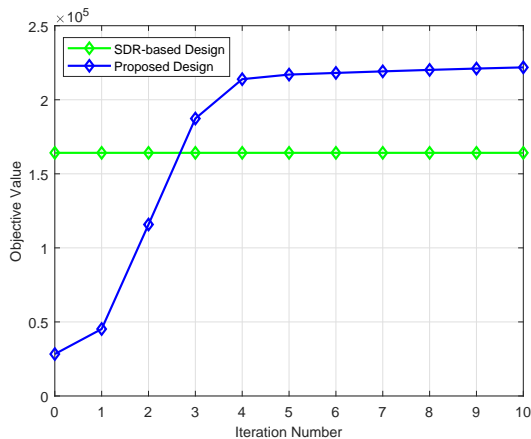


Fig. 5. The convergence of the pilot optimization algorithm.

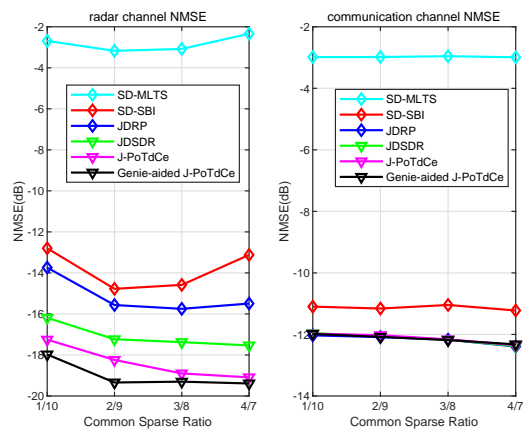


Fig. 6. Channel estimation NMSE versus common sparsity ratio ρ_c .

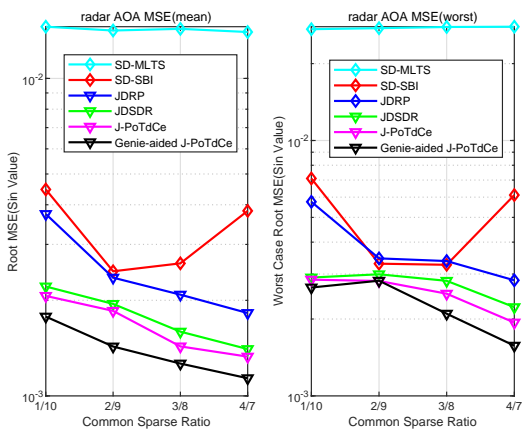


Fig. 7. Average and worst-case MSE of the target AoA versus common sparsity ratio ρ_c .

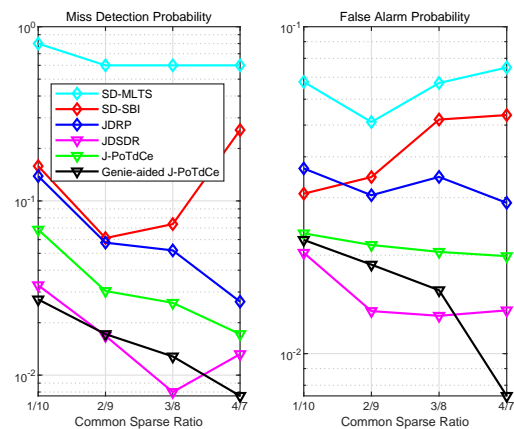


Fig. 8. False alarm probability and miss detection probability versus common sparsity ratio ρ_c .

B. Impact of Common Sparsity Ratio

In Fig. 6 - 8, we compare the parameter estimation and target detection performance versus the common sparsity ratio ρ_c , respectively. It can be seen that the joint design achieves a better overall performance than the separate design. Moreover, as ρ_c increases, the performance gap between the joint design and separate design increases in general. This shows that the joint design approach can exploit the joint sparsity between the radar and communication channels to enhance the estimation/detection performance. Note that however, the radar estimation/detection

performance itself does not necessarily improve with ρ_c because the statistics (AoAs) of the radar channel also changes with ρ_c . The proposed J-PoTdCe can achieve a better performance than all practical baseline schemes (i.e., excluding the genie-aided J-PoTdCe) for any given ρ_c , due to the exploitation of the joint burst sparsity as well as the optimization of pilot. Note that the performance gap between the proposed J-PoTdCe and genie-aided J-PoTdCe is small, which verifies the feasibility of pilot optimization based on the estimated information in Stage 1.

VI. CONCLUSION

We proposed a two-stage joint pilot optimization, target detection and channel estimation scheme to exploit the pilot beamforming gain and joint burst sparsity of ISAC channels for enhanced target detection and channel estimation performance. In Stage 1, the BS performs joint target detection and channel estimation based on the reflected omnidirectional DP and received UP signals. In Stage 2, the BS exploits the prior information obtained in Stage 1 to optimize the DP signal to achieve beamforming gain and further refine the detection/estimation performance. Specifically, a Turbo-SBI algorithm, which is a generalization of the Turbo-OAMP in [27] from the PO measurement matrix to arbitrary measurement matrix with dynamic grid parameters, has been proposed for joint target detection and channel estimation in both stages. The pilot optimization problem in Stage 2 is formulated as a worst-case CRB minimization problem, which contains non-smooth rank-1 constraints. By replacing each rank-1 constraint with a tight and smooth approximation, we developed an efficient pilot optimization algorithm based on the MM method. Simulations verified that the proposed scheme can achieve significant gain over baseline schemes.

APPENDIX

A. Message Update Equations for Module B of Turbo-SBI

1) Message Passing Over the Path $x_m^r \rightarrow f_m^r \rightarrow s_m^r \rightarrow \eta_m^r \rightarrow s_m$:

The message from variable node x_m^r to factor node f_m^r is

$$\nu_{x_m^r \rightarrow f_m^r}(x_m^r) = \mathcal{CN}(x_m^r; x_{B,m}^{r,pr_i}, v_{B,m}^{r,pr_i}). \quad (45)$$

The message from factor node f_m^r to variable node s_m^r is

$$\begin{aligned} \nu_{f_m^r \rightarrow s_m^r}(s_m^r) &\propto \int \nu_{x_m^r \rightarrow f_m^r}(x_m^r) \times f_m^r(x_m^r, s_m^r) dx_m^r \\ &\propto \pi_{s_m^r, m}^{in} \delta(s_m^r - 1) + (1 - \pi_{s_m^r, m}^{in}) \delta(s_m^r), \end{aligned} \quad (46)$$

where $\pi_{s_m^r, m}^{in} = (1 + \frac{\mathcal{CN}(0; x_{B,m}^{r, pri}, v_{B,m}^{r, pri})}{\mathcal{CN}(0; x_{B,m}^{r, pri}, v_{B,m}^{r, pri} + (\sigma_m^r)^2)})^{-1}$. Then the message from variable node s_m^r to factor node η_m^r is the same as $\nu_{f_m^r \rightarrow s_m^r}(s_m^r)$. The message from factor node η_m^r to variable node s_m is

$$\begin{aligned} \nu_{\eta_m^r \rightarrow s_m}(s_m) &= \sum_{\mathbf{s}^r} \eta_m^r(s_m^r, s_m) \times \nu_{s_m^r \rightarrow \eta_m^r}(s_m^r) \\ &= \pi_{s, m}^{r, in} \delta(s_m - 1) + (1 - \pi_{s, m}^{r, in}) \delta(s_m), \end{aligned} \quad (47)$$

where $\pi_{s, m}^{r, in} = (1 + \frac{1 - \pi_{s^r, m}^{in}}{1 + 2\pi_{s^r, m}^{in} \rho^r - \pi_{s^r, m}^{in} - \rho^r})^{-1}$.

2) The message passing over the path $x_m^c \rightarrow f_m^c \rightarrow s_m^c \rightarrow \eta_m^c \rightarrow s_m$ is similar to that in 1) and thus is omitted for conciseness. The final result is given by

$$\nu_{\eta_m^c \rightarrow s_m}(s_m) = \pi_{s, m}^{c, in} \delta(s_m - 1) + (1 - \pi_{s, m}^{c, in}) \delta(s_m), \quad (48)$$

where $\pi_{s, m}^{c, in} = (1 + \frac{1 - \pi_{s^c, m}^{in}}{1 + 2\pi_{s^c, m}^{in} \rho^c - \pi_{s^c, m}^{in} - \rho^c})^{-1}$ and $\pi_{s^c, m}^{in} = (1 + \frac{\mathcal{CN}(0; x_{B,m}^{c, pri}, v_{B,m}^{c, pri})}{\mathcal{CN}(0; x_{B,m}^{c, pri}, v_{B,m}^{c, pri} + (\sigma_m^c)^2)})^{-1}$.

3) Message Passing Over the Markov Chain of \mathbf{s} :

$$\nu_{h_m \rightarrow s_m}(s_m) \propto \gamma_m^f s_m + (1 - \gamma_m^f)(1 - s_m), \quad (49)$$

$$\nu_{h_{m+1} \rightarrow s_m}(s_m) \propto \gamma_m^b s_m + (1 - \gamma_m^b)(1 - s_m), \quad (50)$$

where

$$\gamma_m^f = \frac{\rho_{0,1}(1 - \pi_{m-1}^{in})(1 - \gamma_{m-1}^f) + \rho_{1,1}\pi_{m-1}^{in}\gamma_{m-1}^f}{(1 - \pi_{m-1}^{in})(1 - \gamma_{m-1}^f) + \pi_{m-1}^{in}\gamma_{m-1}^f}, \quad (51)$$

$$\gamma_m^b = \frac{\rho_{1,0}((\pi_{R,m}^{in})^{-1} - 1)((\gamma_{m+1}^b)^{-1} - 1) + (1 - \rho_{1,0})}{(\rho_{0,0} + \rho_{1,0})((\pi_{m+1}^{in})^{-1} - 1)((\gamma_{m+1}^b)^{-1} - 1) + \rho_{1,1} + \rho_{0,1}}, \quad (52)$$

with $\gamma_1^f = \frac{\rho_{0,1}}{\rho_{0,1} + \rho_{1,0}}$, $\gamma_M^b = \frac{1}{2}$ and $\pi_m^{in} = \frac{\pi_{s,m}^{r, in} \pi_{s,m}^{c, in}}{\pi_{s,m}^{r, in} \pi_{s,m}^{c, in} + (1 - \pi_{s,m}^{r, in})(1 - \pi_{s,m}^{c, in})}$.

4) Message Passing Over the Path $s_m \rightarrow \eta_m^r \rightarrow s_m^r \rightarrow f_m^r \rightarrow x_m^r$:

The message from variable node s_m to factor node η_m^r is

$$\begin{aligned}
\nu_{s_m \rightarrow \eta_m^r}(s_m) &\propto \nu_{h_m \rightarrow s_m}(s_m) \times \nu_{h_{m+1} \rightarrow s_m}(s_m) \times \nu_{\eta_m^c \rightarrow s_m}(s_m) \\
&= \pi_{s,m}^{r,out} \delta(s_m - 1) + (1 - \pi_{s,m}^{r,out}) \delta(s_m),
\end{aligned} \tag{53}$$

where $\pi_{s,m}^{r,out} = \frac{\gamma_m^f \gamma_m^b}{\gamma_m^f \gamma_m^b + ((\pi_{s,m}^{c,in})^{-1} - 1)(1 - \gamma_m^f)(1 - \gamma_m^b)}$. The message from factor node η_m^r to variable node s_m^r is

$$\begin{aligned}
\nu_{\eta_m^r \rightarrow s_m^r}(s_m^r) &\propto \sum_{s_m} \eta_m^r(s_m^r, s_m) \times \nu_{s_m \rightarrow \eta_m^r}(s_m) \\
&= \pi_{s^r,m}^{out} \delta(s_m^r - 1) + (1 - \pi_{s^r,m}^{out}) \delta(s_m^r),
\end{aligned} \tag{54}$$

where $\pi_{s^r,m}^{out} = \pi_{s,m}^{r,out} \rho^r$. The message from variable node s_m^r to the factor node f_m^r is the same as $\nu_{\eta_m^r \rightarrow s_m^r}(s_m^r)$. The message from variable node f_m^r to factor node x_m^r is

$$\begin{aligned}
\nu_{f_m^r \rightarrow x_m^r}(s_m^r) &= \sum_{s_m^r} \nu_{\eta_m^r \rightarrow s_m^r}(s_m^r) \times f_m^r(x_m^r, s_m^r) \\
&= \pi_{s^r,m}^{out} \mathcal{CN}(x_m^r; 0, (\sigma_m^r)^2) + (1 - \pi_{s^r,m}^{out}) \delta(x_m^r).
\end{aligned} \tag{55}$$

5) The message passing over $s_m \rightarrow \eta_m^c \rightarrow s_m^c \rightarrow f_m^c \rightarrow x_m^c$ is similar to that in 4).

B. Proof of Lemma 1

The rank of a positive semi-definite matrix $\mathbf{V} \in \mathbb{C}^{M \times M}$ is given by

$$\text{rank}(\mathbf{V}) = \sum_m u(\lambda_m) \tag{56}$$

where $\{\lambda_m\}_{m=1}^M$ denote the eigenvalues of \mathbf{V} and $u(x)$ denotes the step-function. It is easy to see that

$$u(\lambda_m) = \frac{\log\left(1 + \frac{\lambda_m}{\varepsilon}\right)}{\log\left(1 + \frac{1}{\varepsilon}\right)} + o(\varepsilon), \tag{57}$$

where $\lim_{\varepsilon \rightarrow 0} o(\varepsilon) = 0$. Therefore, we have

$$\begin{aligned}
\text{rank}(\mathbf{V}) &= \sum_m \frac{\log\left(1 + \frac{\lambda_m}{\varepsilon}\right)}{\log\left(1 + \frac{1}{\varepsilon}\right)} + o(\varepsilon) \\
&= \frac{M \log\left(\frac{1}{\varepsilon}\right) + \log(|\mathbf{V} + \varepsilon \mathbf{I}|)}{\log\left(1 + \frac{1}{\varepsilon}\right)} + o(\varepsilon)
\end{aligned} \tag{58}$$

Moreover, for any given $\varepsilon > 0$, the RHS of (41) is a concave function of \mathbf{V} since $\log|\mathbf{V} + \varepsilon\mathbf{I}|$ is a concave function of \mathbf{V} .

REFERENCES

- [1] F. Liu, C. Masouros, A. P. Petropulu, H. Griffiths, and L. Hanzo, "Joint radar and communication design: Applications, state-of-the-art, and the road ahead," *IEEE Transactions on Communications*, vol. 68, no. 6, pp. 3834–3862, 2020.
- [2] Z. Feng, Z. Fang, Z. Wei, X. Chen, Z. Quan, and D. Ji, "Joint radar and communication: A survey," *China Communications*, vol. 17, no. 1, pp. 1–27, 2020.
- [3] O. B. Akan and M. Arik, "Internet of radars: Sensing versus sending with joint radar-communications," *IEEE Communications Magazine*, vol. 58, no. 9, pp. 13–19, 2020.
- [4] B. Paul, A. R. Chiriyath, and D. W. Bliss, "Survey of rf communications and sensing convergence research," *IEEE Access*, vol. 5, pp. 252–270, 2017.
- [5] J. Wang, X. Liang, L. Chen, L. Wang, and K. Li, "First demonstration of joint wireless communication and high-resolution sar imaging using airborne mimo radar system," *IEEE Transactions on Geoscience and Remote Sensing*, vol. 57, no. 9, pp. 6619–6632, 2019.
- [6] C. Shi, F. Wang, S. Salous, and J. Zhou, "Joint subcarrier assignment and power allocation strategy for integrated radar and communications system based on power minimization," *IEEE Sensors Journal*, vol. 19, no. 23, pp. 11 167–11 179, 2019.
- [7] Y. Liu, G. Liao, J. Xu, Z. Yang, and Y. Zhang, "Adaptive ofdm integrated radar and communications waveform design based on information theory," *IEEE Communications Letters*, vol. 21, no. 10, pp. 2174–2177, 2017.
- [8] M. Jamil, H. Zepernick, and M. I. Pettersson, "On integrated radar and communication systems using oppermann sequences," in *MILCOM 2008 - 2008 IEEE Military Communications Conference*, 2008, pp. 1–6.
- [9] T. Huang, N. Shlezinger, X. Xu, Y. Liu, and Y. C. Eldar, "Majorcom: A dual-function radar communication system using index modulation," *IEEE Transactions on Signal Processing*, vol. 68, pp. 3423–3438, 2020.
- [10] W. Zhang, S. Vedantam, and U. Mitra, "Joint transmission and state estimation: A constrained channel coding approach," *IEEE Transactions on Information Theory*, vol. 57, no. 10, pp. 7084–7095, 2011.
- [11] M. Kobayashi, H. Hamad, G. Kramer, and G. Caire, "Joint state sensing and communication over memoryless multiple access channels," in *2019 IEEE International Symposium on Information Theory (ISIT)*, 2019, pp. 270–274.
- [12] P. Kumari, S. A. Vorobyov, and R. W. Heath, "Adaptive virtual waveform design for millimeter-wave joint communication-radar," *IEEE Transactions on Signal Processing*, vol. 68, pp. 715–730, 2020.
- [13] F. Liu, C. Masouros, T. Ratnarajah, and A. Petropulu, "On range sidelobe reduction for dual-functional radar-communication waveforms," *IEEE Wireless Communications Letters*, vol. 9, no. 9, pp. 1572–1576, 2020.
- [14] F. Liu, C. Masouros, A. Li, H. Sun, and L. Hanzo, "Mu-mimo communications with mimo radar: From co-existence to joint transmission," *IEEE Transactions on Wireless Communications*, vol. 17, no. 4, pp. 2755–2770, 2018.
- [15] W. Yuan, F. Liu, C. Masouros, J. Yuan, D. W. K. Ng, and N. González-Prelcic, "Bayesian predictive beamforming for vehicular networks: A low-overhead joint radar-communication approach," *IEEE Transactions on Wireless Communications*, vol. 20, no. 3, pp. 1442–1456, 2021.
- [16] A. Liu, V. Lau, and W. Dai, "Joint burst lasso for sparse channel estimation in multi-user massive mimo," in *2016 IEEE International Conference on Communications (ICC)*, 2016, pp. 1–6.
- [17] L. Gaudio, M. Kobayashi, G. Caire, and G. Colavolpe, "On the effectiveness of ofts for joint radar parameter estimation and communication," *IEEE Transactions on Wireless Communications*, vol. 19, no. 9, pp. 5951–5965, 2020.

- [18] Z. Gao, L. Dai, Z. Wang, and S. Chen, "Spatially common sparsity based adaptive channel estimation and feedback for FDD massive MIMO," *IEEE Trans. Signal Processing*, vol. 63, no. 23, pp. 6169–6183, Dec. 2015.
- [19] X. Rao and V. Lau, "Compressive sensing with prior support quality information and application to massive MIMO channel estimation with temporal correlation," *IEEE Trans. Signal Processing*, vol. 63, no. 18, pp. 4914–4924, Sept. 2015.
- [20] M. Masood, L. Afify, and T. Al-Naffouri, "Efficient coordinated recovery of sparse channels in massive MIMO," *IEEE Trans. Signal Processing*, vol. 63, no. 1, pp. 104–118, Jan. 2015.
- [21] X. Rao and V. K. Lau, "Distributed compressive CSIT estimation and feedback for FDD multi-user massive MIMO systems," *IEEE Trans. Signal Processing*, vol. 62, no. 12, pp. 3261–3271.
- [22] A. Liu, V. K. N. Lau, and W. Dai, "Exploiting burst-sparsity in massive mimo with partial channel support information," *IEEE Transactions on Wireless Communications*, vol. 15, no. 11, pp. 7820–7830, 2016.
- [23] Z. Gao, L. Dai, W. Dai, B. Shim, and Z. Wang, "Structured compressive sensing-based spatio-temporal joint channel estimation for FDD massive MIMO," *IEEE Trans. Commun.*, vol. 64, no. 2, pp. 601–617, Feb 2016.
- [24] L. Gaudio, M. Kobayashi, G. Caire, and G. Colavolpe, "Joint radar target detection and parameter estimation with mimo ofts," in *2020 IEEE Radar Conference (RadarConf20)*, 2020, pp. 1–6.
- [25] F. Liu, Y.-F. Liu, A. Li, C. Masouros, and Y. C. Eldar, "Cramér-rao bound optimization for joint radar-communication design," *arXiv preprint arXiv:2101.12530*, 2021.
- [26] E. Tzoreff and A. J. Weiss, "Single sensor path design for best emitter localization via convex optimization," *IEEE Transactions on Wireless Communications*, vol. 16, no. 2, pp. 939–951, 2017.
- [27] A. Liu, L. Lian, V. K. N. Lau, and X. Yuan, "Downlink channel estimation in multiuser massive mimo with hidden markovian sparsity," *IEEE Transactions on Signal Processing*, vol. 66, no. 18, pp. 4796–4810, 2018.
- [28] 3GPP, "Technical Specification Group Services and System Aspects; Release 15 Description; Summary of Rel-15 Work Items (Release 15)," 3rd Generation Partnership Project (3GPP), Technical Report (TR) 21.915, 12 2018, v0.5.0. [Online]. Available: <https://www.3gpp.org/release-15>
- [29] Z. Gao, L. Dai, S. Han, C.-L. I, Z. Wang, and L. Hanzo, "Compressive sensing techniques for next-generation wireless communications," *IEEE Wireless Communications*, vol. 25, no. 3, pp. 144–153, 2018.
- [30] J. Vila and P. Schniter, "Expectation-maximization Bernoulli-Gaussian approximate message passing," in *Signals, Systems and Computers (ASILOMAR), 2011 Conference Record of the Forty Fifth Asilomar Conference on*. IEEE, 2011, pp. 799–803.
- [31] M. Bayati and A. Montanari, "The dynamics of message passing on dense graphs, with applications to compressed sensing," *IEEE Trans. Info. Theory*, vol. 57, no. 2, pp. 764–785, Feb 2011.
- [32] S. Som and P. Schniter, "Compressive imaging using approximate message passing and a markov-tree prior," *IEEE Trans. Signal Processing*, vol. 60, no. 7, pp. 3439–3448, July 2012.
- [33] J. Ma, X. Yuan, and L. Ping, "Turbo compressed sensing with partial DFT sensing matrix," *IEEE Signal Processing Letters*, vol. 22, no. 2, pp. 158–161, 2015.
- [34] S. M. Kay, *Fundamentals of statistical signal processing: estimation theory*. Prentice-Hall, Inc., 1993.